Pharm Res (2015) 32:1741–1751
DOI 10.1007/s11095-014-1572-3

RESEARCH PAPER

Rifampicin Loaded Mannosylated Cationic Nanostructured Lipid Carriers for Alveolar Macrophage-specific Delivery

Xu Song • Qing Lin • Ling Guo • Yao Fu • Jianfeng Han • Huan Ke • Xun Sun • Tao Gong • Zhirong Zhang

Received: 11 July 2014 / Accepted: 10 November 2014 / Published online: 19 November 2014

ABSTRACT

Purpose In this study, cationic mannosylated nanostructured lipid carriers (Man-NLCs) were developed for the targeted delivery of rifampicin to alveolar macrophages.

Methods Rifampicin loaded Man-NLCs (RFP-Man-NLCs) and rifampicin loaded unmodified nanostructured lipid carriers (REP-NLCs) were prepared using thin film homogenization method and characterized by particle size, polydispersity index, zeta potential, transmission electron microscopy, encapsulation efficiency, pharmacokinetics, biodistribution, cell specific targeting, cytotoxicity and inflammatory response.

Results RFP-Man-NLCs and REP-NLCs obtained displayed a size distribution around 160 nm (PDI <0.30) with positive charges of approximately 30 mV. The encapsulation efficiency of RFP was above 90%. In the biodistribution study, both RFP-Man-NLCs and RFP-NLCs, compared with the commercially available rifampicin solution, displayed superior lung-targeting ability. Compared to REP-NLCs, RFP-Man-NLCs exhibited significantly higher uptake efficiency in NR8383 cells and alveolar macrophages, which achieved cell-specific targeting. In addition, RFP-Man-NLCs were demonstrated to be a safe formulation with minimum toxicity and no inflammatory response.

Conclusions RFP-Man-NLCs provided an alternative strategy for selectively delivering rifampicin to alveolar macrophages.

KEY WORDS alveolar macrophages · cationic nanostructured lipid carriers · mannosylation · rifampicin

X. Song • Q. Lin • L. Guo • Y. Fu • J. Han • H. Ke • X. Sun • T. Gong (✉) • Z. Zhang (✉)
Key Laboratory of Drug Targeting and Drug Delivery Systems, Ministry of Education, Sichuan University, Chengdu, People's Republic of China
e-mail: gongtaoy@126.com
e-mail: zrzzl@vip.sina.com

ABBREVIATIONS

AMs	Alveolar macrophages
AUC	Area under the curve
CLz	Plasma clearance
C_{max}	maximum concentration
DAPI	4′,6-diamidino-2-phenylindole
DDAB	Dimethyldioctadecylammonium bromide
DMSO	Dimethyl sulfoxide
EPC	Purified ovolecithin
FITC-DHPE	Fluorescein isothiocyanate labeled DHPE
MCT	Medium chain triglyceride
MRT	Mean retention time
MTT	3-[4, 5-dimethylthiazol-2-yl]-2, 5-diphenyltetrazolium bromide
OCT	Octadecylamine
PDI	Polydispersity index
REP-NLCs	Rifampicin loaded nanostructured lipid carriers
RFP	Rifampicin
RFP Solution	Rifampicin commercial solution
RFP-Man-NLCs	Cationic mannosylated rifampicin nanostructured lipid carriers
$t_{1/2z}$	Half-life
TEM	Transmission electron microscopy

INTRODUCTION

Tuberculosis (TB), a common respiratory infectious disease, presents serious threats to public health. Each year, TB infects 2.5–3.2 million population worldwide which results in about 3 million deaths (1,2). Accounting for more than 80% of all TB cases, pulmonary TB is characterized by the participation of alveolar macrophages (AMs) harboring a large number of M. tuberculosis (3). Intracellular parasites such as M. tuberculosis are taken up by AMs *via* phagocytosis and secrete molecules

which could protect them from phagosome-lysosome fusion (4). AMs thus become incubators for TB which resists digestion by lysosomal enzyme (5–7). Mycobacterium tuberculosis (MTB), hidden in AMs, often stages a comeback and leads to secondary tuberculosis (5).

To produce a significant antibacterial effect against MTB, effective concentration of antibiotics, higher than the minimum inhibitory concentration, is often required (8). Clinically, antibiotics are generally administered by the oral and parenteral route for the treatment of TB. Accordingly, antibiotics mostly likely distribute nonspecifically to tissues or organs *via* the systemic circulation, undesirable effects are thus frequently induced (9–11). Moreover, the amount of antibiotics that accumulate in AMs is insufficient to efficiently inhibit the delitescent MTB. Hence, it is urgent to develop a new delivery system of antibiotics for improving the therapeutic efficacy while minimizing side effects.

Recently, cationic drug delivery vectors, such as cationic polymer, proteins and lipids, have been widely used in gene delivery and tumor specific drug delivery (12). Cationic vectors were shown to interact with negatively charged complexes and serum components *via* "opsonization effect", which results in a rapid elimination from the blood circulation (13). Nevertheless, this effect was confirmed as an alternative strategy for lung targeting, which is based on the filtering effect of capillary beds (14–16). Microparticles with sizes larger than the pore size of pulmonary capillaries may achieve selective accumulation at the lung, thus providing a unique opportunity to treat lung disorders (17,18).

To treat the intracellular MTB in AMs, antibiotics loaded nanoparticle systems targeting to AMs have been extensively studied in the past years (8,9,19–21). The sugar modified nanoscale vectors appeared to be a promising platform system in the targeted delivery of antibiotics to AMs (8). Mannose receptors were demonstrated to be specifically expressed on the AM surfaces, which have high affinity with mannose terminal molecules (22). In addition, the study on the interaction between AMs and different sugar-modified derivatives found that α-D-mannose derivatives can be rapidly adsorbed by AMs (22). Therefore, using α-D-mannosylated NLCs as carriers for antibiotics may increase the cellular uptake by AMs.

In the study, we developed a mannosylated nanostructured lipid carrier system for specific delivery of antibiotics to AMs for TB treatment. Rifampicin, a first-line antibiotics for TB, was loaded in mannosylatged NLCs and unmodified NLCs. The biodistribution profiles of both formulations were investigated to evaluate the lung targeting efficiency. Cell specific targeting was further confirmed by intracellular uptake in NR8383 cells *in vitro* and AMs *via* intravenous administration. The toxicity and inflammatory response of REP-Man-NLCs were further assessed *in vitro* and *in vivo*.

MATERIALS AND METHODS

Rifampicin (RFP) was obtained from HongJing Chemical Co., Ltd (Hubei, China). Purified ovolecithin (EPC) (purity 80%) was purchased from Lipoid GmbH (Ludwigshafen, Germany). Medium chain triglyceride (MCT) was purchased from Beiya Medical oil CO., Ltd (Tieling, China). Octadecylamine (OCT) was offered by Shengke (Shengke Chemical Co, Ltd, Jining, China). Dimethyldioctadecylammonium bromide (DDAB) and mannan were obtained from Sigma-Aldrich (USA). Fluorescein isothiocyanate (FITC) labeled DHPE was offered by Invitrogen (Carlsbad, CA, USA). The 3-[4, 5-dimethylthiazol-2-yl]-2, 5-diphenyltetrazolium bromide (MTT) and trypsin were obtained from Sigma Chemical Co. (St. Louis, MO). All other chemicals were of analytical reagent grade or better.

Cell Lines and Animals

NR8383 and L929 cell lines were purchased from Shanghai Institutes for Biological Sciences (SIBS; Shanghai, China). Wistar rats were provided by the Experimental Animal Center of Sichuan University (Chengdu, China). Institute of Cancer Research (ICR) mice were supplied by Chengdu Dossy biological technology Co., Ltd (Chengdu, China). All the animal experiments were approved by the Institutional Animal Care and Ethic Committee (People's Republic of China).

Synthesis of Mannosylated Cholesterol Derivative

The mannosylated cholesterol derivative (Man-C6-Chol) was synthesized as previously described (23).

Preparation of RFP-NLCs and REP-Man-NLCs

RFP-NLCs and RFP-Man-NLCs were prepared by thin film homogenization method (24). RFP, EPC, MCT, OCT and DDAB (mass ratio: 2:10:6:1:10) were dissolved in chloroform. The organic solvent was completely evaporated at 40°C under vacuum to form the film, which was then hydrated in water solution. Subsequently, NLCs were obtained by ultrasonic probe at 200 W for 4 min. The mannose coating was carried out in the first step of preparation by adding Man-C6-Chol into the lipid matrix at a molar ratio of 5% (8,23). FITC-labeled RFP-NLCs and RFP-Man-NLCs were prepared similarly by adding 1% FITC-DHPE (w/w) into the formulation.

Characterization of RFP-NLCs and RFP-Man-NLCs

The particle size, polydispersity index (PDI) and zeta potential of both RFP-NLCs and RFP-Man-NLCs, were measured in water at 25°C by dynamic light scattering (Zetasizer Nano ZS90, Malvern Instruments Ltd, Worcestershire, UK). The morphology of both RFP-NLCs and RFP-Man-NLCs, freshly

prepared and stained with 1% (w/v) phosphotungstic acid, was viewed and photographed using a transmission electron microscopy (TEM, H-600, Hitachi, Japan). The encapsulation efficiency of RFP-NLCs and RFP-Man-NLCs was determined using ultra filtration method (25). Nanosep® Centrifugal Filtration Devices (Mw cut-off 300 kDa; PALL Life Science, USA) was utilized to separate the free Rifampicin from the NLCs solution. The collected filtrate, *i.e.* unencapsulated rifampicin (W_u) was diluted with methanol by 100 times and quantified by an ultraviolet spectrophotometer at the wavelength of 474 nm. The equivalent total rifampicin in the nanoparticles (W_t) was measured by the same method. The encapsulation efficiency was calculated as follows: encapsulation efficiency=$(1\text{-}W_u/W_t)\times 100\%$.

Pretreatment and Analysis of Rifampicin in Plasma and Tissue

The plasma and tissue samples were treated as previously described (26). Samples (100 μL) and carbamazepine (8 μL, 1 mg/mL) were mixed and 150 μL acetonitrile was added for protein precipitation. After centrifugation at 11,000*g* for 5 min, 20 μL the supernatant was directly injected for HPLC analysis.

The prepared samples were determined by high performance liquid chromatography (HPLC) which consisted of a reverse-phase column (C_{18}, 250×4.6 mm, 5 μm) with a security guard column (C18, 10×4 mm, 5 μm). The columns were kept at 35°C. The mobile phase consisted of methanol–water (67:33, v/v). The flow rate was maintained at 0.6 mL/min and the detection wavelength was set at 333 nm.

Using afore-mentioned HPLC method condition, there was no endogenous peaks interfering with RFP or carbamazepine. In addition, RFP peaks can be separated well from carbamazepine peaks without any interference. The linear standard curve showed good linearity over the concentration range of 0.1–12 μg/mL. This method then applied to the pharmacokinetic and biodistribution studies of RFP.

Pharmacokinetics in Rat Plasma

Wistar rats (male, 200±20 g) were randomly divided into three groups (n=5). After fasted but had free access to water over 12 h, the three groups were given the commercial drug solution (RFP Solution), RFP-NLCs and RFP-Man-NLCs *via* tail veins injection with a dose equivalent of 5 mg/kg rifampicin, respectively (27). 0.3 mL blood samples were collected at 5, 15, 30, 45, 60, 120, 240, 360, 480, 720 min post injection and centrifuged at 5000*g* for 10 min to obtain 100 μL plasma for HPLC analysis (9,26).

Biodistribution Studies in Mice

To evaluate the delivery efficiency of RFP-NLCs and RFP-NLCs *in vivo*, FITC-labeled RFP-NLCs and REP-Man-NLCs were intravenously injected into ICR mice. 30, 60, 120 and 240 min after injection, mice were immediately sacrificed for intact major organs collection. The fluorescence signals were recorded with *in vivo* imaging system (Quick View 3000, Bio-Real, Austria).

For quantitative determination of RFP, ICR mice (male, 20±5 g) were randomly assigned into three groups (n=5). The mice were fasted but watered for 12 h and were injected with RFP Solution, RFP-NLCs and RFP-Man-NLCs at a dose of 7.2 mg/kg, respectively (27). Blood and tissues, including brain, liver, lung, heart, spleen and kidney, were collected at 30, 60, 120 and 240 min post injection. Tissue samples, based on weight, were added with two volumes of 0.9% NaCl solution and homogenized. 100 μL plasma or tissue samples were collected for HPLC analysis (9,26).

Interaction of RFP-NLCs and REP-Man-NLCs with Serum (16)

RFP-NLCs and RFP-Man-NLCs were mixed with murine serum (1:5, v/v). Turbidity of the mixture were determined by the Varioskan Flash (Thermo Scientific, USA) at a wavelength of 600 nm at the indicated times. Serum alone served as blank control. For morphology evaluation of the aggregates, after mixing RFP-Man-NLCs with murine serum, samples were observed using TEM as described before.

In Vitro Uptake Study in NR8383 Cells

The cellular uptake study was carried out as previously reported (23,28,29). In brief, NR8383 cells were seeded on culture plates for 24 h in the complete medium and switched to serum free medium for 1 h before treated with FITC-labeled RFP-NLCs and RFP-Man-NLC. Then, 20 μL FITC-labeled RFP-NLCs and REP-Man-NLCs were added and incubated for 1 h at 37 or 4°C. One of the groups at the temperature of 37°C was preconditioned with 0.125 mg/mL mannan for 30 min prior to the addition of FITC-labeled RFP-NLCs and REP-Man-NLCs. After treatment, cells were washed three times with phosphate-buffered saline (PBS) and analyzed by flow cytometry using a Cytomics FC500 (Beckman Coulter, USA). In addition, compared with serum free medium, cell uptake in the complete medium at 37°C was also studied as described above.

In Vivo Uptake Experiments in Rats

Wistar rats (male, 200±20 g) were randomly divided into three groups (n=5). The animals in RFP-NLCs group and REP-Man-NLCs group were injected with FITC-labeled RFP-NLCs and REP-Man-NLCs, respectively. For the inhibition study, the animals in mannan group were intratracheally instilled with mannan (5 mg/kg) before the

injection of FITC-labeled RFP-Man-NLCs(8). At 2 h, AMs were collected according to the protocol previously reported and subjected to flow cytometry analysis (8,30).

For qualitative analysis, the lungs were collected 2 h after administration. After fixed in paraformaldehyde (4%), cryosections of the lungs were prepared, and stained with DAPI for fluorescence imaging (Quick View 3000, Bio-Real, Austria). Besides, AMs from three treatment groups were collected as described above and processed for fluorescence imaging.

Cytotoxicity Assay

After seeded in 96-well culture plates for 24 h, L929 cells were treated with RFP-NLCs and RFP-Man-NLCs with various DDAB concentrations ($n=3$) in 100 μL serum-free medium. 1 h later, samples were replaced with fresh complete medium, followed by a further incubation for 20 h. The cytotoxicity was assessed by MTT assay (16). Cell viability was calculated as the following expression: Cell viability = (Absorbance of cells exposed to RFP-NLCs or REP-Man-NLCs)/ (Absorbance of blank cells cultured without any drug) × 100%.

Inflammatory Response Assay

ICR mice (male, 20 ± 5 g) were randomly assigned into four groups ($n=5$). Three groups were injected with RFP Solution, RFP-NLCs and RFP-Man-NLCs at a dose equivalent of 7.2 mg/kg, respectively. Additionally, lipopolysaccharide (LPS, 30 μg per mouse) was used as a positive control. Serum were collected after 2 h and evaluated for the concentration of IL-6 using ELISA kit (R&D systems, USA) at 450 nm. For histological evaluation, lungs and livers were collected at 24 h after injection and fixed in 10% (v/v) formaldehyde. After embedded in paraffin, the samples were cut and stained with hematoxylin-eosin (H&E) for analysis.

Statistical Analysis

All experiments were repeated at least three times. Data were expressed as mean ± SD and analyzed by DAS 2.0 (Mathematical Pharmacology Professional Committee of China, Shanghai, China) for non-linear regression analysis. After the analysis of Student's *t*-test of the two groups, a p value <0.05 was considered to be statistically significant.

RESULTS

Characterization of RFP-NLCs and RFP-Man-NLCs

As shown in Table I, the size and zeta potential of RFP-NLCs and RFP-Man-NLCs showed no significant differences. NLCs displayed a size distribution around 160 nm (PDI <0.30) with positive charges of approximately 30 mV. The encapsulation efficiency of RFP was above 90%. Furthermore, TEM images of RFP-NLCs and RFP-Man-NLCs presented that the particles were round and uniform with particle size ranged from 100 nm to 200 nm, which was in accordance with the DLS measurement (Fig. 1).

Pharmacokinetics in Rat Plasma

The mean plasma concentration–time curves of RFP after intravenous administration of RFP Solution, RFP-NLCs and RFP-Man-NLCs to rats were shown in Fig. 2. The results indicated that RFP Solution, RFP-NLCs and RFP-Man-NLCs shared the same trend. The main pharmacokinetic parameters in rats did not exhibit statistically significant differences among three groups (Table II) ($p>0.05$), indicating that the three formulations were bioequivalent.

Biodistribution Studies in Mice

To investigate the delivery efficiency of RFP-NLCs and RFP-Man-NLCs *in vivo*, the fluorescence of major organs was shown in Fig. 3a. FITC-labeled RFP-NLCs and REP-Man-NLCs were notably accumulated in the lung at the indicated time points. About 4 h after injection, the fluorescence intensity in the lung appeared to decrease and liver accumulation started to increase over time.

Quantitative determination of RFP in major organs was shown in Fig. 3d. As for RFP-Man-NLCs, the concentration of RFP in the lung was 10.48 times at 30 min, 5.81 times at 60 min, 9.17 times at 120 min, and 3.34 times at 240 min higher than that of RFP solution. Moreover, the distribution in kidney decreased compared to that of RFP solution. On the contrary, the distribution in heart exhibited a slight increase. The concentration of RFP in liver, spleen and plasma showed no significant differences among the three groups.

The passive lung targeting of cationic vectors may be attributed to serum-induced aggregation. The turbidity of RFP-NLCs and RFP-Man-NLCs mixed with murine serum was time-dependent (Fig. 3b). The turbidity increased gradually and reached the maximum in 1 h, indicating aggregation happened upon mixing RFP-NLCs and RFP-Man-NLCs with murine serum. After 1 h, the decrease of the turbidity revealed a dissociation of RFP-NLCs and RFP-Man-NLCs with murine serum. In addition, REP-Man-NLCs and murine serum formed complexes, which were typically observed by TEM. Figure 3c showed a loose structure of NLC-serum complexes with a size ranged from 1 to 2 μm, which may result in an efficient retention of RFP-Man-NLCs in the lung capillaries.

Table I Characterization of RFP-NLCs and RFP-Man-NLCs. Data Represent Mean ± S.D. (n =3)

	Size (nm)	PDI	Zeta potential (mV)	Encapsulation efficiency (%)
RFP-NLCs	167.0 ± 2.3	0.243 ± 0.002	31.8 ± 1.4	96.6 ± 0.3
RFP-Man-NLCs	157.4 ± 0.7	0.244 ± 0.008	34.3 ± 1.3	91.6 ± 2.3

Cell Uptake of RFP-Man-NLCs and RFP-NLCs *In Vitro* and *In Vivo*

NR8383 AMs derived from bronchio-alveolar lavage of a normal male SD rats, are a continuous cell line (31). To evaluate the potency of targeted delivery of RFP-Man-NLCs to NR8383 cells, the cell internalization of fluorescently labeled NLCs was determined using flow cytometry. The quantified mean fluorescence intensity (MFI), indicated that intracellular uptake of RFP-Man-NLCs was significantly higher (2.6-fold) than that of RFP-NLCs (p <0.01) at 37°C (Fig. 4a). Intracellular uptake of RFP-Man-NLCs also dramatically exceeded that of RFP-NLCs in the complete medium. However, the introduction of mannan (0.125 mg/ mL) significantly decreased the intracellular uptake of RFP-Man-NLCs (p <0.01). At 4°C, cell binding efficiency of RFP-Man-NLCs and RFP-NLCs (p >0.05) showed no significant differences. Besides, the cellular uptake of RFP-Man-NLCs and RFP-NLCs was temperature-sensitive.

To verify the cell target ability of RFP-Man-NLCs *in vivo*, AMs were isolated at 2 h after intravenous administration in mice. Compared with RFP-NLCs, RFP-Man-NLCs significantly increased the uptake in AMs by 3 fold (Fig. 4b). Furthermore, the inhibition of mannose receptor (mannan) dramatically decreased the uptake of RFP-Man-NLCs by 5 fold. Cryosections of lungs (Fig. 4c) and isolated AMs (Fig. 4d) also confirmed fluorescence accumulation in AMs in the RFP-Man-NLCs treated group.

Cytotoxicity and Inflammatory Response

To evaluate the safety of RFP-Man-NLCs, L929 cells in 100 μL serum-free medium were seeded in 96-well plates and treated with RFP-NLCs and RFP-Man-NLCs with various DDAB concentrations. Obvious cytotoxicity was observed when the concentration of DDAB increased to 18 μg/mL, which was much higher than the concentration used in the *in vitro* uptake study (10 μg/mL) (Fig. 5a). Moreover, DDAB was shown to induce a significant cell death at a concentration of 27 μg/mL with a relative cell viability of less than 70% (Fig. 5a).

To evaluate the inflammatory response, the serum concentration of IL-6 was used as the indicator for RFP-NLCs and RFP-Man-NLCs induced immune responses *in vivo* (Fig. 5b). Results showed no obvious upregulation of cytokines was found after *i.v.* injection of RFP-NLCs, RFP-Man-NLCs and RFP solution in ICR mice. On the contrary, lipopolysaccharide (LPS) strongly induced IL-6 expression (p <0.01). In addition, the histological evaluation of lung and liver sections from four experimental groups showed no inflammatory or pathological changes (Fig. 5c). According to IL-6 results, the histopathological damage caused by LPS was observed microscopically as indicated by mild inflammatory cell infiltration in hepatic lobules.

DISCUSSION

Rifampicin, as the first choice drug, was widely used in the treatment of tuverculosis. To develop rifampicin delivery systems that could facilitate the selective shuttling of drugs to the site of tuberculosis infection, novel delivery devices have been characterized by researchers in recent years, such as liposomal

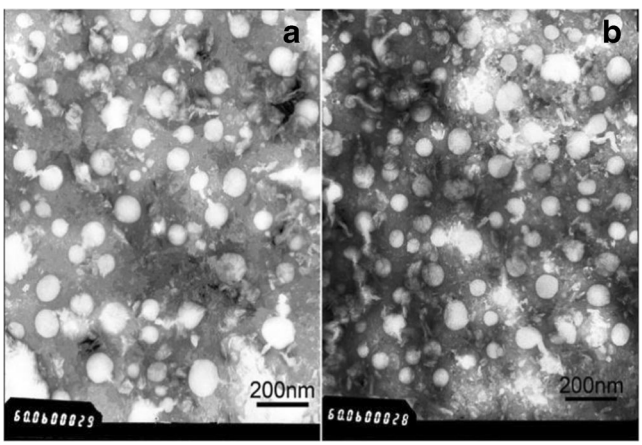

Fig. 1 Transmission electron micrograph images. A. RFP-NLCs; B. REP-Man-NLCs. Scale bar: 200 nm.

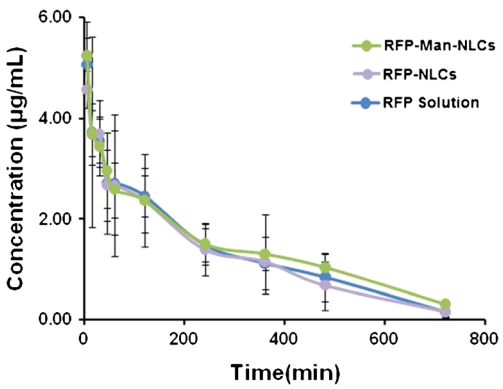

Fig. 2 Mean plasma concentration-time curve of RFP after intravenous injection of RFP Solution, RFP-NLCs and RFP-Man-NLCs in rats (equivalent to 5 mg/kg RFP). Data represent mean ± SD (n =5).

Table II Pharmacokinetic Parameters of RFP Solution, RFP-NLCs and RFP-Man-NLCs. Data Represent Mean ± S.D. ($n = 5$)

Parameters	RFP-NLCs	RFP-Man-NLCs	RFP Solution
$AUC_{(0-t)}(\mu g \cdot mL^{-1} \cdot min)$	1140.4 ± 224.9	962.4 ± 115.0	984.8 ± 82.6
$AUC_{(0-\infty)}(\mu g \cdot mL^{-1} \cdot min)$	1232.4 ± 203.6	1072.4 ± 169.5	1168.0 ± 145.5
$MRT_{(0-t)}(min)$	233.6 ± 5.3	218.9 ± 25.7	223.7 ± 27.2
$MRT_{(0-\infty)}(min)$	297.3 ± 65.2	304.2 ± 135.4	368.7 ± 127.8
$C_{max}(\mu g \cdot mL^{-1})$	5.5 ± 0.4	4.6 ± 0.2	5.2 ± 0.6
$t_{1/2z}(min)$	180.9 ± 86.5	200.5 ± 105.0	274.5 ± 117.2
$CLz(mL \cdot min^{-1} \cdot g)$	16.6 ± 2.9	19.0 ± 3.0	17.3 ± 2.1

aerosols, solid lipid nanoparticles, biodegradable polymeric nanoparticles (4,9,32,33). The present study reported the successful delivery of RFP loaded Man-cationic NLCs to AMs *via* intravascular administration for the first time.

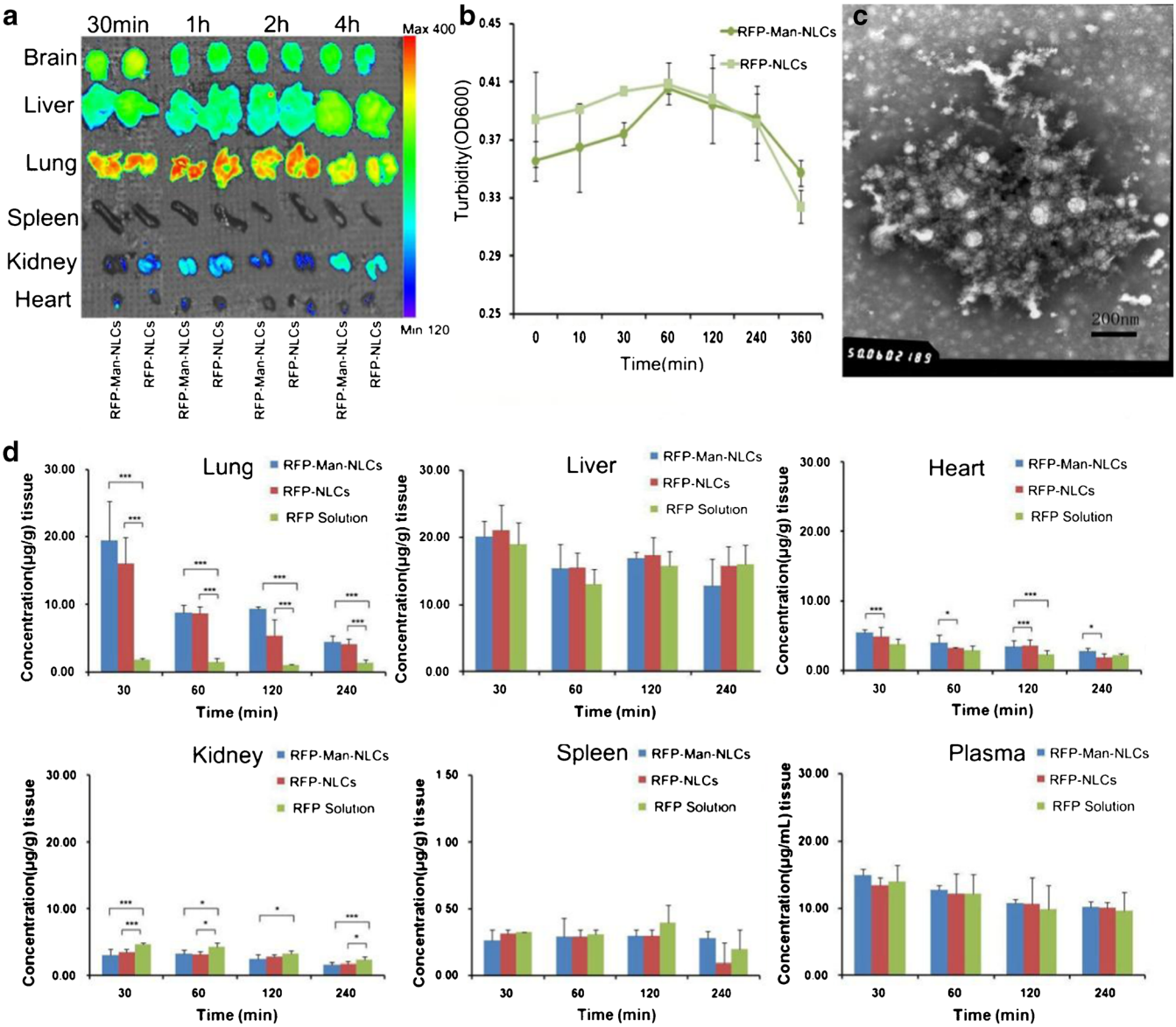

Fig. 3 RFP-Man-NLCs mediated lung accumulation of RFP *in vivo*. (**a**) Representative *in vivo* fluorescence image of major organs of FITC-labeled RFP-NLCs and RFP-Man-NLCs from mice. (**b**) Dynamic changes in the turbidity of RFP-NLCs and RFP-Man-NLCs incubated with murine serum. (**c**) TEM images of the aggregate complex of RFP-Man-NL Cs interacted with serum protein. Scale bar: 200 nm (**d**). Tissue distribution in mice after intravenous injection of RFP Solution, RFP-NLCs and RFP-Man-NLCs in rats. Data represent mean ± S.D. ($n = 5$). *i.v.* 7.2 mg/kg. *$p < 0.05$; ***$p < 0.01$.

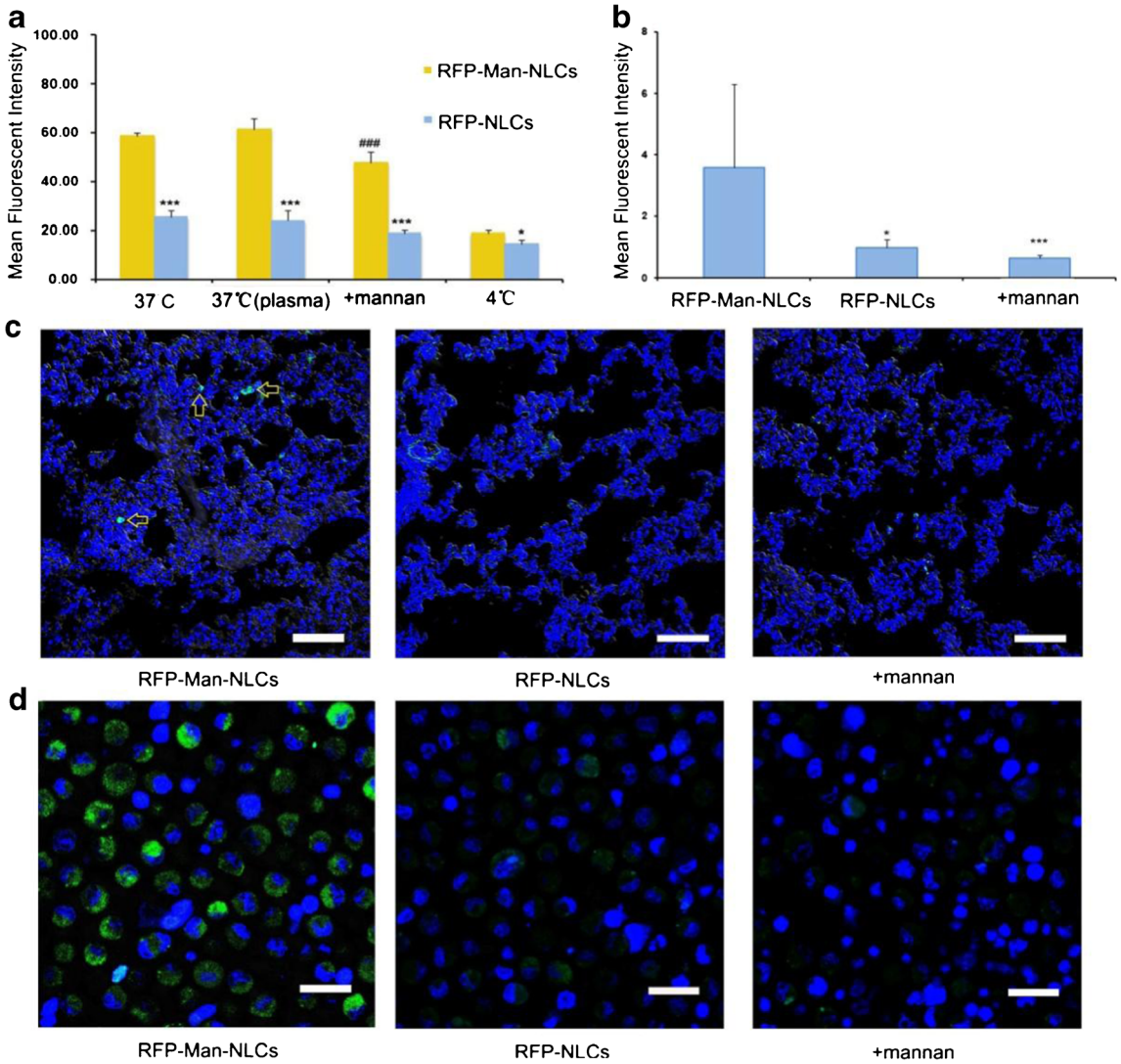

Fig. 4 Cell uptake of RFP-Man-NLCs and RFP-NLCs *in vitro* and *in vivo*. (**a**) Binding and uptake of RFP-Man-NLCs and RFP-NLCs by NR8383 Cells after 1 h incubation at either 4°C or 37°C. ($n = 3$). (**b**) Flow cytometry analysis showing uptake of RFP-Man-NLCs and RFP-NLCs by alveolar macrophages after intravenous administration in rats ($n = 5$). (**c**) Confocal laser scanning microscopy images of lungfrozen sections after intravenous administration in rats. Scale bars represent 100 μm. *Arrows* indicate cell uptake by alveolar macrophages *in vivo*. (**d**) Confocal laser scanning microscopy images of isolated alveolar macrophages after intravenous administration in rats. Scale bars represent 20 μm. Green fluorescence as FITC-labeled RFP-Man-NLCs and RFP-NLCs and blue fluorescence as DAPI observed by confocal laser scanning microscope, as well as the merged image were shown. *$p < 0.05$, ***$p < 0.01$, RFP-Man-NLCs compared with RFP-NLCs. ###$p < 0.01$, RFP-Man-NLCs compared with + mannan.

Mannosylated NLCs were fabricated using DDAB and octadecylamine. The fabrication of NLCs were shown to have following advantages such as the absence of organic solvents, large-scale production, low toxicity, improvement of drug incorporation and controlled release properties by adding spatially incompatible liquid lipids (34,35). Herein, the proposed schematic model is shown in Fig. 6. To achieve high rifampicin encapsulation efficiency, the addition of octadecylamine was necessary which contained a long fatty chain and an ammonium group acting as a bridge linking drugs with the acid group (36). Rifampicin had a phenolic hydroxyl group with weak acidity, which could interact with octadecylamine *via* ionic bonds. Thereby, rifampicin, with high lipophicity, could be encapsulated in NLC carriers with high efficiency. In addition, DDAB, as a commonly used cationic material, was used in fabricating NLCs to introduce cationic properties to the NLCs and to improve the distribution of drug in the lung. Mannosylated cholesterol (Man-C6-Chol), which could insert into the NLCs *via* cholesterol residues, was used to modify NLCs to accomplish cell-specific targeting. In brief, we prepared cationic NLCs with an original size distribution around 100 nm and a zeta potential of about 30 mV.

Interactions between cationic vectors and serum components were reported to be a complex process which might influence the *in vivo* fate of drug cargo (16). In this study, the

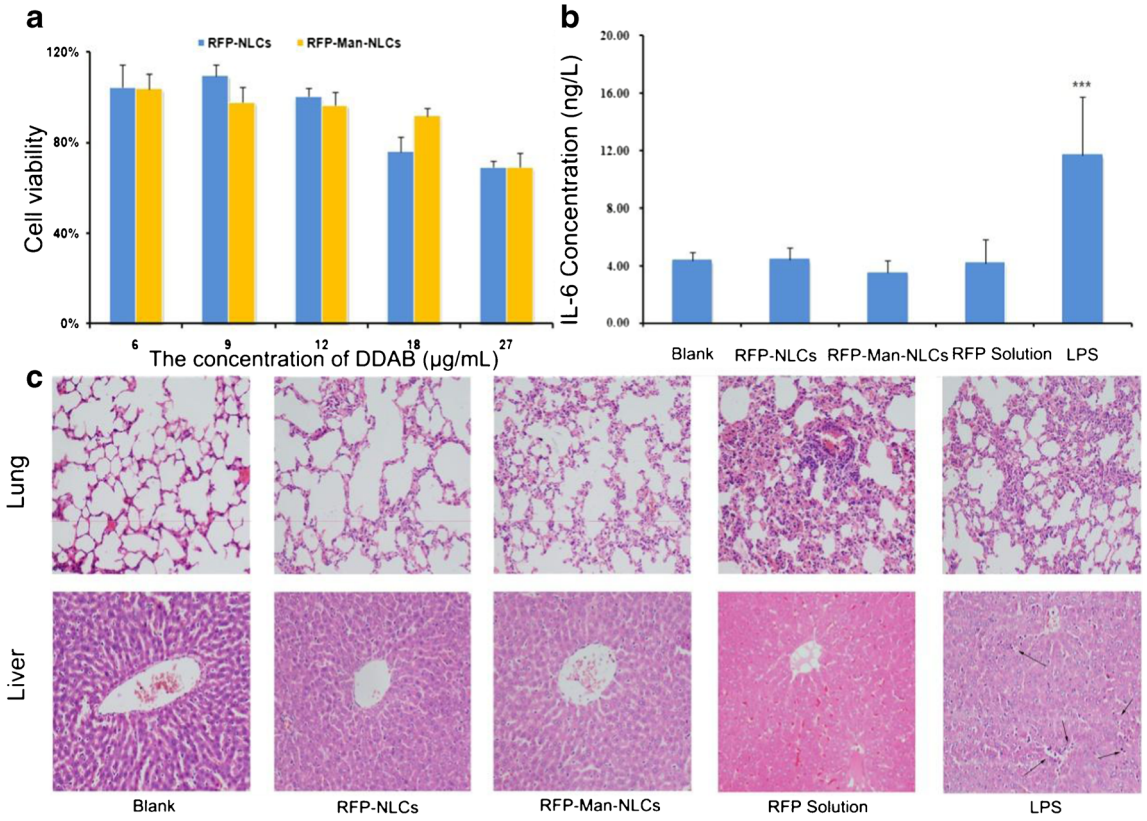

Fig. 5 Relatively low toxicity and immunogenicity of RFP-NLCs and RFP-Man-NLCs. (**a**) MTT assay showed the cytotoxicity of RFP-NLCs and RFP-Man-NLCs. L929 cells were seeded in 96-well cell plate at a cell density of 1×10^5/well for 1 d before treated with RFP-NLCs and RFP-Man-NLCs with various DDAB concentration ($n = 3$) in serum free medium (100 μL). ***$p < 0.01$ indicates the concentration of DDAB, up to 18 μg/mL, reflected significantly cytotoxity. (**b**) IL-6 concentration of mouse serum after *i.v.* injection of RFP-NLCs, RFP-Man-NLCs and RFP-Solution to ICR mice, serum was collected and tested for IL-6 level by ELISA method with Lipopolysaccharide (LPS) (30 μg per mouse) as positive control ($n = 5$). ***$p < 0.01$, compared with LPS group. (**c**) Histological evaluation of lung and liver after *i.v.* injection of RFP-NLCs, RFP-Man-NLCs and RFP Solution (100×). *Arrows* indicate mild inflammatory cell infiltration in hepatic lobules.

aggregation behavior between cationic vectors and serum components occurred rapidly after adding RFP-Man-NLCs and RFP-NLCs to murine serums. 1~2 μm NLC-serum complexes with a hydrophilic protein shell were shown to be retained in pulmonary capillaries thus inducing a rapid accumulation of RFP in the lung tissue as verified by both fluorescence image and HPLC analysis. Generally, particles with size over 7~8 μm could be retained by lung capillary beds (37,38). In addition, particles with smaller sizes, *e.g.* 1~2 μm liposomes, were also proven to achieve lung

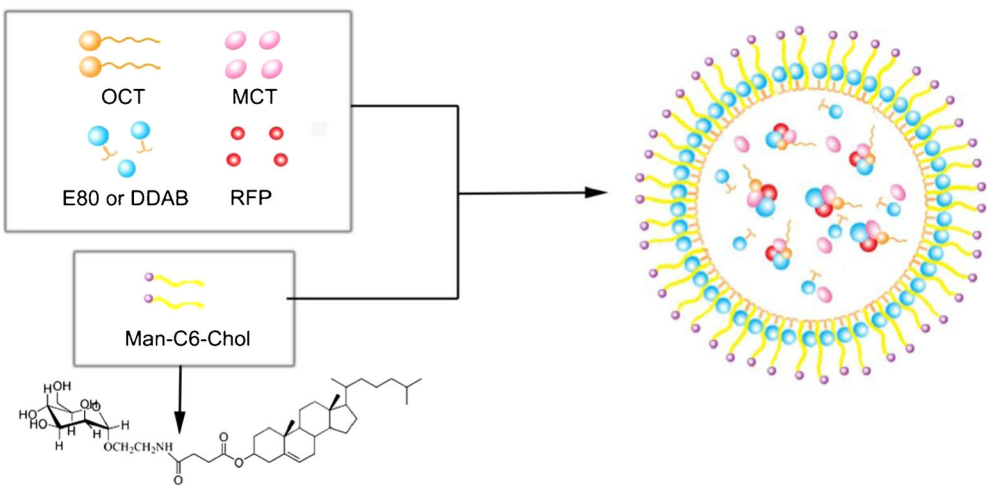

Fig. 6 Structure model diagram of REP-Man-NLCs.

accumulation (39,40). According to the "Vroman-effect" as previously observed on solid lipid nanoparticles, the protein adsorption and desorption is a dynamic process during which proteins with higher abundance and low affinity could be displaced by less abundant proteins with higher affinity (41,42). A dissociation of NLCs and serum complexes could be triggered by the higher affinity proteins contained in serum. After 1 h incubation, the decrease in the turbidity revealed the destabilization of complexes. Therefore, we proposed that once injected into mouse tail vain, RFP-Man-NLCs interacted with serum proteins thus generating large and loose complexes which resulted in the specific accumulation in the lung. Moreover, these complexes might undergo disintegration as triggered by higher affinity proteins. As a result, the ligand of RFP-Man-NLCs would be exposed thus achieving AMs targeting *via* mannose receptor mediated uptake (Fig. 4b, c and d). However, a small proportion of RFP was likely to be released in the blood stream that could be rapidly metabolized in liver and excreted in kidney (Fig. 3d). Also, cationic nano carriers were reported to be eliminated rapidly from blood circulation (13,43,44). For pharmacokinetic studies, no significant differences were observed in the pharmacokinetic behaviors among groups administrated with RFP-Man-NLCs, RFP-NLCs or RFP Solution. The *in vivo* distribution study of nano carriers by fluorescent labeling was proven an efficient and convenient method. FITC-PE used in this study represented NLCs but free RFP which was not encapsulated in the NLCs or released from the NLCs in the blood. Hence, FITC-labeled RFP-NLCs and RFP-Man-NLCs could be detected to stand for most of RFP capsulated in the nano carriers (16). RFP, released from the NLCs, was detected in most major organs according to the quantitative determination of RFP by HPLC. In addition, RFP-Man-NLCs and RFP-NLCs significantly improved the lung accumulation of RFP in comparison with RFP solution (Fig. 3d), while RFP solution displayed no tissue selectivity with most drugs accumulating in the liver which might induce severe liver toxicity (45). Consequently, lower doses of RFP-Man-NLCs and RFP-NLCs could be used to decrease nonspecific distribution in off-target organs including liver while achieving comparable level of accumulation at the target site compared to RFP solution.

AMs were found to be the incubators and hideout of *Mycobacterium*, and thus, it is important for delivery systems to selectively shuttle drugs to the site of infection in lung (9). In the *in vitro* uptake study, RFP-Man-NLCs exhibited specific targeting to NR8383 cells as expected. The cellular uptake of RFP-Man-NLCs that surpassed NLCs without mannosylation could be inhibited by the addition of free mannan. Also, a significantly higher level of cellular uptake of RFP-Man-NLCs at 37°C was observed as compared to 4°C, which indicated that the cellular uptake of RFP-Man-NLCs was energy-dependent endocytosis mediated by the interaction between mannose and corresponding receptors (28,29). In addition, cell uptake in the complete medium did not change the cell-specific targetability, which indicated that the interaction between cationic vectors and serum proteins did not affect the AM targetability of RFP-Man-NLCs. This result could explain the efficient targeting to AMs of RFP-Man-NLCs *in vivo*. A continuous absorption and dissociation of RFP-Man-NLCs and serum complexes may help expose Mannose-residuals which could primarily contact with AM surface receptors thus leading to an efficient cellular delivery.

The safety of RFP-Man-NLCs and RFP-NLCs were evaluated by cytotoxicity and inflammatory response. Despite the cytotoxicity of RFP-Man-NLCs and RFP-NLCs slightly increased along with the rising of the concentration of DDAB, RFP-Man-NLCs and RFP-NLCs were still low toxic vectors for rifampicin delivery. In our study, especially in cell uptake experiments, the concentration was within the low toxicity range. In addition, unlike traditional microspheres with solid structure, the aggregation complexes formed by interaction of RFP-Man-NLCs and RFP-NLCs with serum components were loose and dynamic possessing "Vroman effect", as discussed above (41,42). Morphological assessments and tissue histology of lungs and livers revealed no inflammation and celluler damage induced by NLCs, comfirmed by Fig. 5c and d. These results revealed that RFP-Man-NLCs and RFP-NLCs accumulation occurred in the lung without inducing inflammatory response, thus suggesting that RFP-Man-NLCs and RFP-NLCs are not toxic under these conditions.

CONCLUSION

In summary, we designed and developed mannosylated cationic nanostructured lipid carriers for AM targeted delivery of rifampicin. When administered systemically, cationic RFP-Man-NLCs were demonstrated to interact with serum proteins and form NLC-protein complexes with significantly larger sizes which exhibited a primary lung accumulation. Furthermore, RFP-Man-NLCs exhibited AM targetability both *in vitro* and *in vivo*. The optimized RFP-Man-NLCs formulation was proven to have minimum cytotoxicity which was safe for systemic administration. Our results demonstrated that RFP-Man-NLCs could be a promising carrier for the treatment of delitescent TB.

ACKNOWLEDGMENTS AND DISCLOSURES

This work was funded by the National S&T Major Project of China (Grant No. 2012ZX09304004001) and the National

Basic Research Program of China (No. 2013CB932504). The authors report no conflicts of interest.

REFERENCES

1. Aal AMA, El-Mashad N, Magdi D. Tuberculosis problem in Dakahlia Governorate, Egypt. SAARC J Tuberc Lung Dis HIV/AIDS. 2013;10:43–9.
2. Fauci AS. Infectious diseases: considerations for the 21st century. Clin Infect Dis. 2001;32:675–85.
3. Bermudez LE. Use of liposome preparation to treat mycobacterial infections. Immunobiology. 1994;191:578–83.
4. Vyas S, Kannan M, Jain S, Mishra V, Singh P. Design of liposomal aerosols for improved delivery of rifampicin to alveolar macrophages. Int J Pharm. 2004;269:37–49.
5. Natarajan K, Kundu M, Sharma P, Basu J. Innate immune responses to< i> M. tuberculosis</i> infection. Tuberculosis. 2011;91:427–31.
6. McKinney JD, zu Bentrup KH, Muñoz-Elías EJ, Miczak A, Chen B, Chan W-T, *et al.* Persistence of Mycobacterium tuberculosis in macrophages and mice requires the glyoxylate shunt enzyme isocitrate lyase. Nature. 2000;406:735–8.
7. Zahrt TC. Molecular mechanisms regulating persistent< i> Mycobacterium tuberculosis</i> infection. Microbes Infect. 2003;5:159–67.
8. Wijagkanalan W, Kawakami S, Takenaga M, Igarashi R, Yamashita F, Hashida M. Efficient targeting to alveolar macrophages by intratracheal administration of mannosylated liposomes in rats. J Control Release. 2008;125:121–30.
9. Chuan J, Li Y, Yang L, Sun X, Zhang Q, Gong T, *et al.* Enhanced rifampicin delivery to alveolar macrophages by solid lipid nanoparticles. J Nanoparticle Res. 2013;15:1–9.
10. Yee D, Valiquette C, Pelletier M, Parisien I, Rocher I, Menzies D. Incidence of serious side effects from first-line antituberculosis drugs among patients treated for active tuberculosis. Am J Respir Crit Care Med. 2003;167:1472–7.
11. Mohr JF, McKinnon PS, Peymann PJ, Kenton I, Septimus E, Okhuysen PC. A retrospective, comparative evaluation of dysglycemias in hospitalized patients receiving gatifloxacin, levofloxacin, ciprofloxacin, or ceftriaxone. Pharmacother J Hum Pharmacol Drug Ther. 2005;25:1303–9.
12. Shi S, Han L, Gong T, Zhang Z, Sun X. Systemic delivery of microRNA-34a for cancer stem cell therapy. Angew Chem. 2013;125:3993–7.
13. Braeckmans K, Buyens K, Bouquet W, Vervaet C, Joye P, Vos FD, *et al.* Sizing nanomatter in biological fluids by fluorescence single particle tracking. Nano Lett. 2010;10:4435–42.
14. Li S, Tseng W, Stolz DB, Wu S, Watkins S, Huang L. Dynamic changes in the characteristics of cationic lipidic vectors after exposure to mouse serum: implications for intravenous lipofection. Gene Ther. 1999;6:585–94.
15. Ishiwata H, Suzuki N, Ando S, Kikuchi H, Kitagawa T. Characteristics and biodistribution of cationic liposomes and their DNA complexes. J Control Release. 2000;69:139–48.
16. Han J, Wang Q, Zhang Z, Gong T, Sun X. Cationic bovine serum albumin based self assembled nanoparticles as siRNA delivery vector for treating lung metastatic cancer. Small. 2014;10:524–35.
17. Kutscher HL, Chao P, Deshmukh M, Singh Y, Hu P, Joseph LB, *et al.* Threshold size for optimal passive pulmonary targeting and retention of rigid microparticles in rats. J Control Release. 2010;143:31–7.
18. Deshmukh M, Kutscher HL, Gao D, Sunil VR, Malaviya R, Vayas K, et al. Biodistribution and renal clearance of biocompatible lung targeted poly (ethylene glycol)(PEG) nanogel aggregates. J Control Release. 2012;164:65–73.
19. Lawlor C, Kelly C, O'Leary S, O'Sullivan M, Gallagher P, Keane J, *et al.* Cellular targeting and trafficking of drug delivery systems for the prevention and treatment of MTb. Tuberculosis. 2011;91:93–7.
20. Briones E, Isabel Colino C, Lanao JM. Delivery systems to increase the selectivity of antibiotics in phagocytic cells. J Control Release. 2008;125:210–27.
21. Chellat F, Merhi Y, Moreau A, Yahia LH. Therapeutic potential of nanoparticulate systems for macrophage targeting. Biomaterials. 2005;26:7260–75.
22. Largent B, Walton K, Hoppe C, Lee Y, Schnaar R. Carbohydrate-specific adhesion of alveolar macrophages to mannose-derivatized surfaces. J Biol Chem. 1984;259:1764–9.
23. Li P, Chen S, Jiang Y, Jiang J, Zhang Z, Sun X. Dendritic cell targeted liposomes–protamine–DNA complexes mediated by synthetic mannosylated cholestrol as a potential carrier for DNA vaccine. Nanotechnology. 2013;24:295101.
24. Pardeike J, Hommoss A, Müller RH. Lipid nanoparticles (SLN, NLC) in cosmetic and pharmaceutical dermal products. Int J Pharm. 2009;366:170–84.
25. Guo Y, Liu X, Sun X, Zhang Q, Gong T, Zhang Z. Mannosylated lipid nano-emulsions loaded with lycorine-oleic acid ionic complex for tumor cell-specific delivery. Theranostics. 2012;2:1104.
26. Melo L, Queiroz R, Queiroz M. Automated determination of rifampicin in plasma samples by in-tube solid-phase microextraction coupled with liquid chromatography. J Chromatogr B. 2011;879:2454–8.
27. Zhao D, Gao ZD, Han DE, Li N, Zhang YJ, Lu Y, *et al.* Influence of rifampicin on the pharmacokinetics of salvianolic acid B may involve inhibition of organic anion transporting polypeptide (oatp) mediated influx. Phytother Res. 2012;26:118–21.
28. Cui Z, Han S-J, Huang L. Coating of mannan on LPD particles containing HPV E7 peptide significantly enhances immunity against HPV-positive tumor. Pharm Res. 2004;21:1018–25.
29. Hattori Y, Kawakami S, Lu Y, Nakamura K, Yamashita F, Hashida M. Enhanced DNA vaccine potency by mannosylated lipoplex after intraperitoneal administration. J Gene Med. 2006;8:824–34.
30. Chakravarthy KV, Davidson BA, Helinski JD, Ding H, Law W-C, Yong K-T, *et al.* Doxorubicin-conjugated quantum dots to target alveolar macrophages and inflammation. Nanomed Nanotechnol Biol Med. 2011;7:88–96.
31. Jones B, Dickinson P, Gumbleton M, Kellaway I. Lung surfactant phospholipids inhibit the uptake of respirable microspheres by the alveolar macrophage NR8383. J Pharm Pharmacol. 2002;54:1065–72.
32. Diab R, Brillault J, Bardy A, Gontijo AVL, Olivier JC. Formulation and in vitro characterization of inhalable polyvinyl alcohol-free rifampicin-loaded PLGA microspheres prepared with sucrose palmitate as stabilizer: efficiency for ex vivo alveolar macrophage targeting. Int J Pharm. 2012;436:833–9.
33. Hirota K, Hasegawa T, Hinata H, Ito F, Inagawa H, Kochi C, *et al.* Optimum conditions for efficient phagocytosis of rifampicin-loaded PLGA microspheres by alveolar macrophages. J Control Release. 2007;119:69–76.
34. Uner M. Preparation, characterization and physico-chemical properties of solid lipid nanoparticles (SLN) and nanostructured lipid carriers (NLC): their benefits as colloidal drug carrier systems. Die Pharm Int J Pharm Sci. 2006;61:375–86.
35. Müller R, Radtke M, Wissing S. Nanostructured lipid matrices for improved microencapsulation of drugs. Int J Pharm. 2002;242:121–8.
36. Li M, Zheng Y, Shan F-Y, Zhou J, Gong T, Zhang Z-R. Development of ionic-complex-based nanostructured lipid carriers to improve the pharmacokinetic profiles of breviscapine. Acta Pharmacol Sin. 2013;34:1108–15.

37. Illumand L, Davis S. The targeting of drugs parenterally by use of microspheres. PDA J Pharm Sci Technol. 1982;36: 242–8.
38. Rappand R, Bivins B. Final in-line filtration: removal of contaminants from IV fluids and drugs. Hosp Formul. 1983;18:1124–8.
39. Wilkinsand D, Myers P. Studies on the relationship between the electrophoretic properties of colloids and their blood clearance and organ distribution in the rat. Br J Exp Pathol. 1966;47:568.
40. Fidler I, Raz A, Fogler W, Kirsh R, Bugelski P, Poste G. Design of liposomes to improve delivery of macrophage-augmenting agents to alveolar macrophages. Cancer Res. 1980;40:4460–6.
41. Vroman L, Adams A, Fischer G, Munoz P. Interaction of high molecular weight kininogen, factor XII, and fibrinogen in plasma at interfaces. Blood. 1980;55:156–9.
42. Göppertand T, Müller R. Adsorption kinetics of plasma proteins on solid lipid nanoparticles for drug targeting. Int J Pharm. 2005;302: 172–86.
43. Buyens K, Meyer M, Wagner E, Demeester J, De Smedt SC, Sanders NN. Monitoring the disassembly of siRNA polyplexes in serum is crucial for predicting their biological efficacy. J Control Release. 2010;141:38–41.
44. Buyens K, De Smedt SC, Braeckmans K, Demeester J, Peeters L, van Grunsven LA, *et al*. Liposome based systems for systemic siRNA delivery: stability in blood sets the requirements for optimal carrier design. J Control Release. 2012;158:362–70.
45. Tasduq S, Singh K, Satti N, Gupta D, Suri K, Johri R. Terminalia chebula (fruit) prevents liver toxicity caused by sub-chronic administration of rifampicin, isoniazid and pyrazinamide in combination. Hum Exp Toxicol. 2006;25:111–8.